Materials Today Physics 44 (2024) 101451

Contents lists available at ScienceDirect

Materials Today Physics

journal homepage: www.journals.elsevier.com/materials-today-physics

High cooling and power generation performance of α-MgAgSb with intrinsic low lattice thermal conductivity

Xiaofan Zhang [a,b], Nan Chen [a,b], Kaiwei Guo [a,b], Qintuo Zhang [c], Qi Zhao [d], Jingkun Xu [c], Hangtian Zhu [a,**], Huaizhou Zhao [a,*]

[a] Beijing National Laboratory for Condensed Matter Physics, Institute of Physics, Chinese Academy of Sciences, Beijing, 100190, China
[b] College of Materials Science and Opto-Electronic Technology, University of Chinese Academy of Sciences, Beijing, 100049, China
[c] Nuclear Science and Technology, East China University of Technology, Jiangxi, Nanchang, 330013, China
[d] Hebei Key Lab of Optic-Electronic Information and Materials, Key Laboratory of High-Precision Computation and Application of Quantum Field Theory of Hebei Province, College of Physics Science and Technology, Hebei University, Baoding, 071002, China

ARTICLE INFO

Keywords:
α-MgAgSb
Lattice thermal conductivity
Thermoelectric modules
Thermoelectric cooling and power generation

ABSTRACT

α-MgAgSb is a promising near-room temperature thermoelectric material, characterized by its intrinsically low lattice thermal conductivity, a feature attributed to the significant atomic mass contrast and complex crystal structure. In this work, we achieved respective zT_{avg} values of 0.58 in the temperature range of 150–300 K and 1.22 in the range of 300–550 K for α-MgAgSb, indicating exceptional potential for both cooling and power generation applications. Additionally, through the reduction of cross-sectional size, the stability of MgAgSb/Ag interface was enhanced under high temperature, which is crucial for the practical application of thermoelectric module. To verify the property of α-MgAgSb material, a 7-pair MgAgSb/Bi_2Te_3 module was fabricated, demonstrating a maximum cooling temperature difference ΔT_{max} of 60 K at hot-side temperature of 300 K and a power generation efficiency η_{max} of 7.2 % with ΔT of 275 K. This work paves the way for the application of Mg-based thermoelectric materials.

Thermoelectric (TE) cooling, the most significant solid-state cooling technique, is the primary application in the thermoelectric field, offering advantages such as precise temperature control, directional heat transfer, compact structure and quiet operation [1,2]. The crucial parameters such as cooling capacity and efficiency of thermoelectric modules are related to the performance of thermoelectric materials. In particular, the cooling temperature difference is directly determined by the dimensionless figure of merit zT, defined as $zT = \frac{S^2\sigma}{\kappa}T$, where S, σ, κ and T are the Seebeck coefficient, electrical conductivity, thermal conductivity and absolute temperature, respectively [3–5]. Among them, the $S^2\sigma$, named as power factor *PF*, plays a crucial role in the maximum cooling capacity of a thermoelectric module. Bi_2Te_3-based materials have traditionally been the primary option for near-room temperature thermoelectric cooling applications. However, achieving breakthrough in Bi_2Te_3-based modules to increase the cooling temperature difference remains challenging [6–8]. Consequently, the development for novel materials capable of superior performance at room temperature has emerged as a pivotal frontier in thermoelectric research.

In thermoelectric cooling systems, high thermal conductivity can result in undesirable heat and energy loss, significantly contributing to low efficiency of TE modules. Thus, it is essential to develop new thermoelectric materials through establishing new search strategies that focus on materials with low thermal conductivity [9–11]. The thermal conductivity of a material mainly comes from two components: the electronic contribution (κ_e) and the lattice contribution (κ_L). The former can be calculated by the Wiedemann–Franz law, which reveals a proportional relationship with electrical conductivity and temperature. The correlation between electronic thermal conductivity and electrical conductivity, carrier concentration, and Seebeck coefficient contributes to the challenge of optimizing thermoelectric properties through adjustments in electronic thermal conductivity. In contrast, the lattice thermal conductivity is relatively independent of other transport parameters which is dominated by lattice vibrations, *i.e.* the propagation of phonons [12,13]. At room temperature, the Umklapp process is weakened due to the reduced phonon population at high $\hbar\omega$. Therefore, only

* Corresponding author.
** Corresponding author.
E-mail addresses: htzhu@iphy.ac.cn (H. Zhu), hzhao@iphy.ac.cn (H. Zhao).

https://doi.org/10.1016/j.mtphys.2024.101451
Received 25 April 2024; Received in revised form 29 April 2024; Accepted 30 April 2024
Available online 3 May 2024

materials with inherently low lattice thermal conductivity hold potential for near-room temperature applications. Investigating the phonon-induced thermal properties from a structural perspective is crucial in the search for new room temperature thermoelectric materials.

It has been reported that significant mass fluctuations and complex crystal structures are conducive to a low lattice thermal conductivity [14].In this study, the mean deviation of atomic mass is utilized to determine mass fluctuation of materials, and it is defined as $A.D. = \frac{\sum|x-\bar{x}|}{n}$, where x represents the mass of atom in formula, $\bar{x}$ denotes the average atomic mass, and n is the number of atoms in the formula. Additionally, the complexity of the material's crystal structure is determined by counting the atoms (defined as N) within the primitive cell. In this work, the relationships between room-temperature lattice thermal conductivity and the corresponding atomic mass deviation, atoms number within primitive cell for various thermoelectric materials have been summarized, as shown in Fig. 1. The results indicated that thermoelectric materials located within the blue region, such as Mg_2Si [15] , ZrNiSn [16] , SiGe [17] and FeVSb [18] exhibit high lattice thermal conductivity, over 3 W m^{-1} K^{-1}, which can be attributed to the low *A.D.* and *N*, meaning small atomic mass contrast and relatively simple crystal structures. Conversely, for the materials situated in the red region, such as PbTe [19] , Bi_2Te_3 [20] , BiSb [21] and $Mg_3(Bi,Sb)_2$ [22], despite their lower *N* values, low lattice thermal conductivity can still be maintained due to the significant variation in atomic mass. Moreover, as for $Ba_8Ga_{18}Ge_{30}$ material [23] , despite the minimal atomic mass variance, it exhibits a relatively low lattice thermal conductivity, which is largely attributed to the complexity of the crystal structure ($N = 54$).

As a promising substitute to p-type Bi_2Te_3 thermoelectric materials, α-MgAgSb has received extensive attention due to its low lattice thermal conductivity and excellent electrical transport properties [24]. Both plots in Fig. 1 revealed that α-MgAgSb occupies an advantaged position with a high *A.D.* of 40 and *N* of 24 among various thermoelectric materials, exhibiting a low lattice thermal conductivity of 0.58 W m^{-1} K^{-1} at room temperature. This indicates that α-MgAgSb has favorable potential for thermoelectric cooling applications, as its low lattice thermal conductivity can contribute to the promising zT values at near-room temperature.

In this work, α-MgAgSb material was synthesized by a two-step high-energy ball milling and spark plasma sintering method. Powder X-ray diffraction (XRD) result in Fig. S1 showed that there was no significant impurity, meaning phase-pure α-MgAgSb was obtained. Thermoelectric properties of α-MgAgSb at 150–573 K have been characterized and analyzed. The Seebeck coefficient and thermal conductivity at low temperature were measured using TTMS and the electrical resistivity was measured by PPMS [31]. As shown in Fig. 2a, the increasing of electrical resistivity with temperature at 150–348 K showed metallic transport behavior of α-MgAgSb sample. However, the electrical resistivity decreased rapidly when the temperature exceeded 348 K, due to the bipolar effect. The Seebeck coefficient exhibited the same temperature-dependent features as the electrical resistivity, attributed to the charge carrier excitation with increasing temperature. The Goldsmid-Sharp bandgap E_g can be calculated from the maximum Seebeck coefficient and the temperature at which it occurs. The Seebeck coefficient of α-MgAgSb reached the peak value of 251 μV/K at 348 K and the bandgap was 0.28 eV. Combining the electrical resistivity and Seebeck coefficient, a power factor *PF* of 21 μW cm^{-1} K^{-2} was obtained at room temperature, as shown in Fig. 2b. The thermal conductivity first decreased with temperature increasing because of the enhanced Umklapp scattering and then increased due to the bipolar effect. A low thermal conductivity of 0.75 W m^{-1} K^{-1} at room temperature was obtained and the corresponding lattice thermal conductivity was 0.58 W m^{-1} K^{-1}, which was calculated through single parabolic band (SPB) model. The intrinsic low lattice thermal conductivity of α-MgAgSb can be attributed to the high mass contrast and the complex primitive cell, as shown in Fig. 1. The excellent thermoelectric performance of α-MgAgSb at both low and high temperature can be seen in Fig. 2c. The zT value increased with temperature and reached 0.86 at room temperature, which was comparable to the p-type Bi_2Te_3 material [30] , and higher than that of the α-$MgAg_{0.97}Sb_{0.99}$ material [29]. When the temperature exceeded 348 K, the zT of Bi_2Te_3 decreased rapidly due to the bipolar effect while the zT of α-MgAgSb kept increasing and reached a zT_{max} of 1.39 at 523 K, indicating that α-MgAgSb was a potential substitute to Bi_2Te_3 material. In fact, the average performance of thermoelectric materials over the operating temperature range is very important, whether they are used for cooling or power generation application. Fig. 2d showed the respective zT_{avg} values of α-MgAgSb at the temperature range of 150–300 K for thermoelectric cooling and 300–550 K for power generation. The α-MgAgSb material had a zT_{avg} of 0.58 in the temperature range of 150–300 K, close to the 0.64 of Bi_2Te_3. However, in the 300–550 K range, the zT_{avg} of α-MgAgSb was 1.22, surpassing that of commercial Bi_2Te_3 material. The result suggests that α-MgAgSb has the potential to be an effective thermoelectric material over a wide

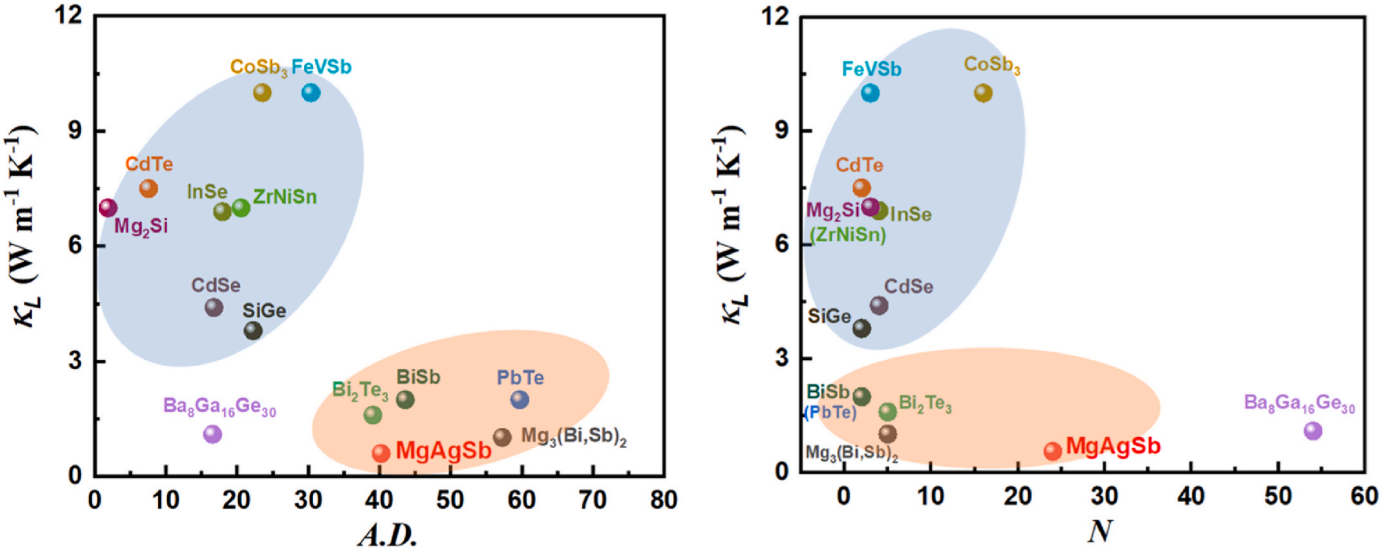

Fig. 1. The lattice thermal conductivity κ_L of various thermoelectric materials as a function of (a) the mean deviation of atomic mass *A.D* [15–23,25–28] and (b) the number of atoms per primitive cell *N*.

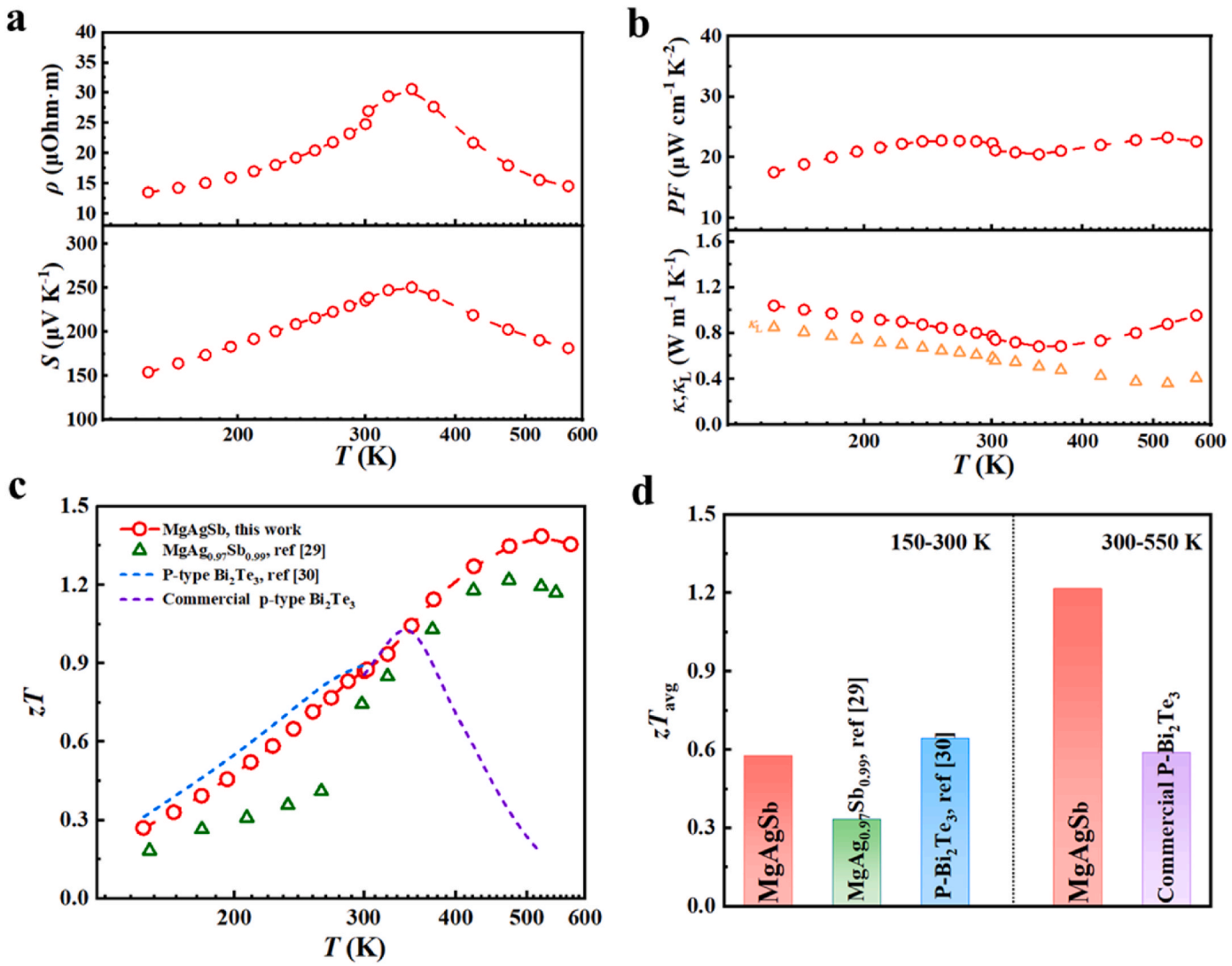

Fig. 2. Temperature dependent TE properties for α-MgAgSb materials. (a) Resistivity and Seebeck coefficient, (b) power factor, thermal conductivity and lattice thermal conductivity, (c) zT value and (d) average zT in comparison to the value of Bi_2Te_3 from commercial and literature results [29,30].

temperature range for both cooling and power generation.

Grain boundaries represent one of the dominant scattering sources for the electrical transport properties of materials at near-room temperature. Increasing the grain size of materials has become a common strategy to enhance carrier mobility and thereby improve the zT values of these materials. To further optimize the room temperature performance, the MgAgSb samples were annealed at 623 K, 673 K and 773 K for 24 h, respectively, followed by a further annealing at 553 K for 72 h in order to make sure that samples were transitioned to α-phase. For convenience, samples annealed at 623 K, 673 K and 773 K were named as S623, S723 and S773, respectively. As shown in Fig. 3a, the XRD results showed that all the annealed samples can maintain pure α-phase. The SEM images showed that all the annealed samples exhibited an average grain size of 2 μm, which was 10 times larger than that of the pristine MgAgSb sample (Fig. S2). And the samples only annealed at 553 K for 72 h (S553) exhibited an average grain size of 200 nm, meaning that the process of annealing at 553 K for 72 h had no influence on grain growth for α-MgAgSb. The electrical and thermal transport properties of annealed α-MgAgSb samples were characterized and these samples exhibited similar thermoelectric performance. As shown in Fig. 3b, the room-temperature resistivity was decreased from 27 μΩ m for pristine α-MgAgSb to 16–17 μΩ m for annealed samples. To our surprise, the decrease of resistivity for annealed samples was mainly due to the increase of the carrier concentration, which changed from 2.88×10^{19} cm^{-3} to 4.9×10^{19} cm^{-3} (Fig. S3). And combined with the enlarged grain size, the mobility of annealed samples was almost unchanged in this work. The Seebeck coefficient of the annealed samples also decreased from 240 μV/K to 200 μV/K due to the increased carrier concentration (Fig. 3c). In spite of this, a high power factor of 24.3 μW cm^{-1} K^{-2} for annealed MgAgSb sample was achieved at room temperature, which was 120 % higher than that of pristine sample (Fig. 3d). As the temperature rising, the difference of resistivity and Seebeck coefficient between the pristine and annealed samples was gradually reduced due to bipolar effect. Although the electrical transport property was enhanced, the thermal conductivity κ also increased ~25 % over the whole temperature range after annealing, which was mainly due to the increased electron thermal conductivity, as shown in Fig. 3e. As a consequence, the zTs of the annealed samples showed a 10 % decline to pristine MgAgSb, as shown in Fig. 3f. The results indicated that annealing process could enhance the electrical transport performance of MgAgSb material, but it also raised the thermal conductivity due to the increased carrier concentration.

In addition to the performance of TE material, the stability of contact also plays a crucial role in TE modules, where attention must be given not only to the bonding strength and element diffusion at the interface but also to the potential cracking during working condition. While the

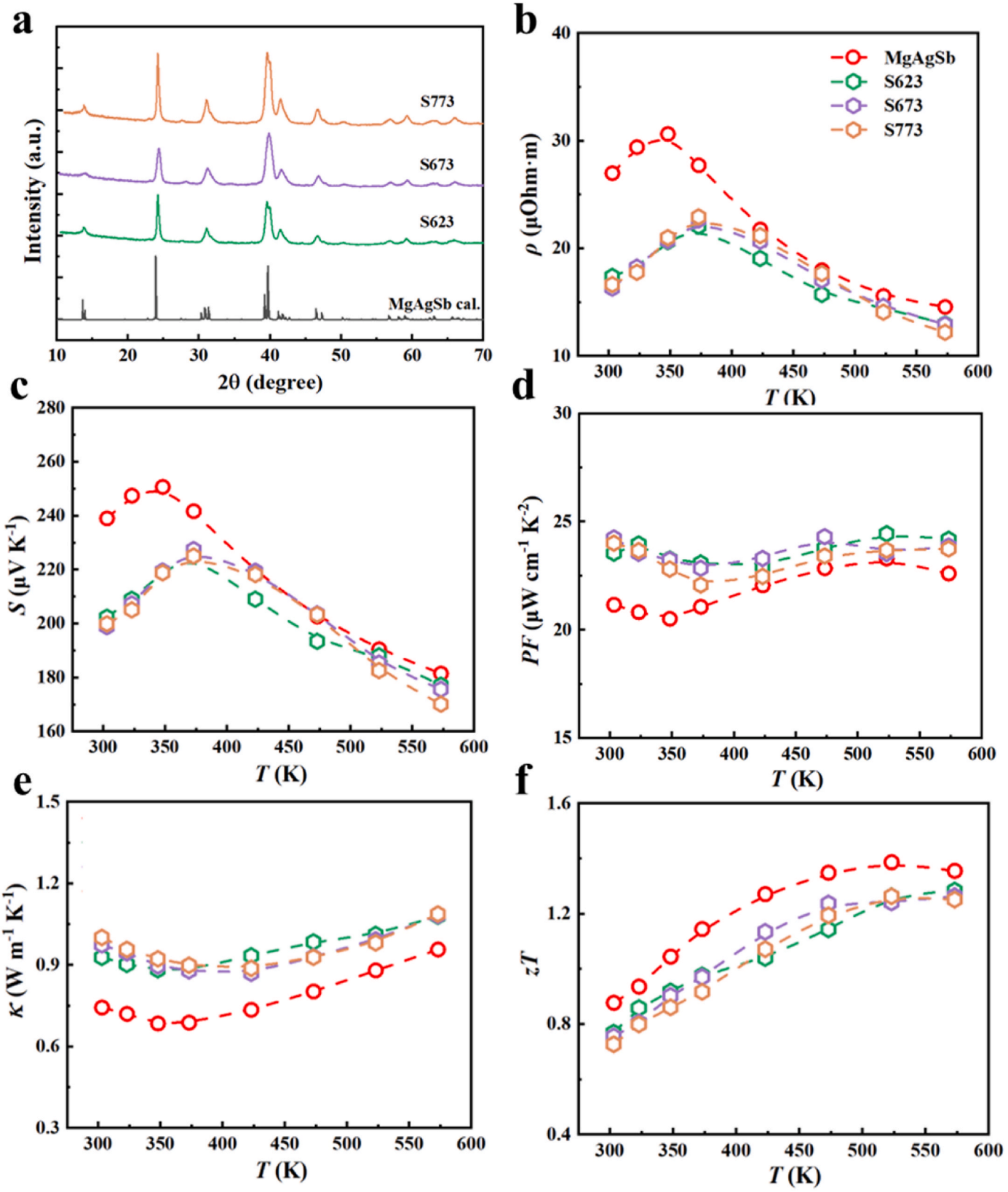

Fig. 3. Phase and TE properties analysis for annealed α-MgAgSb materials. (a) XRD patterns, (b) resistivity, (c) Seebeck coefficient, (d) power factor, (e) thermal conductivity and (f) *zT* value.

Ag electrode is commonly used for the α-MgAgSb material [32], its thermal expansion mismatch can lead to the development of cracks between the Ag electrode layer and the α-MgAgSb material, especially under significant temperature increases [33]. However, mitigating interfacial thermal stresses can be achieved by reducing the cross-sectional areas. To address this issue, we conducted an investigation into the stability of MgAgSb/Ag junctions. Specifically, we annealed MgAgSb/Ag thermoelectric legs with various cross-sectional sizes at 553 K for 12, 24, and 48 h, and subsequently monitored changes in microstructure and interfacial resistivity, as illustrated in Fig. 4. The analysis revealed different contact performance among MgAgSb/Ag thermoelectric legs with various cross-sectional sizes. The MgAgSb/Ag legs with a cross-sectional size of 1.3 × 1.3 mm^2 showed excellent interface integration without crack forming, contrasting with the 3 × 3 and 5 × 5 mm^2 sizes, where cracks emerged obviously. Meanwhile, EDS results showed that there was no element diffusion at the interface between Ag and α-MgAgSb in the above three sizes (Figs. S4–S6). Fig. 4d and Fig. S7 showed the change of contact resistivity with annealing time under different cross-sectional sizes. The contact resistivities of thermoelectric legs with cross-sectional sizes of 3 × 3 mm^2 and 5 × 5 mm^2 increased significantly with annealing time. When the annealing time was 48 h, the contact resistivity increased from ~11 μΩ cm^2 to 417.6 μΩ cm^2 and 635 μΩ cm^2 for the TE legs with cross-sectional sizes of 3 × 3 mm^2 and 5 × 5 mm^2, respectively, resulting from the cracks at the interface. On the contrary, the contact resistivity of the thermoelectric leg with the cross-sectional size of 1.3 × 1.3 mm^2 was almost unchanged with the annealing time increasing. Contact resistivity data indicated that smaller section size can maintain high thermal stability under prolonged annealing process, revealing that the appropriate reduction in cross-sectional dimensions can prevent cracking caused in the high-temperature process.

To verify the properties of the α-MgAgSb material, a 7-pair thermoelectric module based on p-type α-MgAgSb and n-type Bi_2Te_3 with a height of 3 mm was fabricated in this work. The thermoelectric performance of the n-type Bi_2Te_3 material was shown in the Supporting materials (Fig. S8). In order to maximize module performance and facilitate assembly, the cross-sectional sizes of p-type α-MgAgSb and n-type Bi_2Te_3 were 1.3 × 1.3 mm^2 and 1.2 × 1.2 mm^2, respectively. Fig. 5a showed the temperature difference ΔT of MgAgSb/Bi_2Te_3 module as a function of input current. The cooling ΔT increased until it reached a maximum and then dropped with the current increased. The heat flow and temperature distribution in the module were determined by the

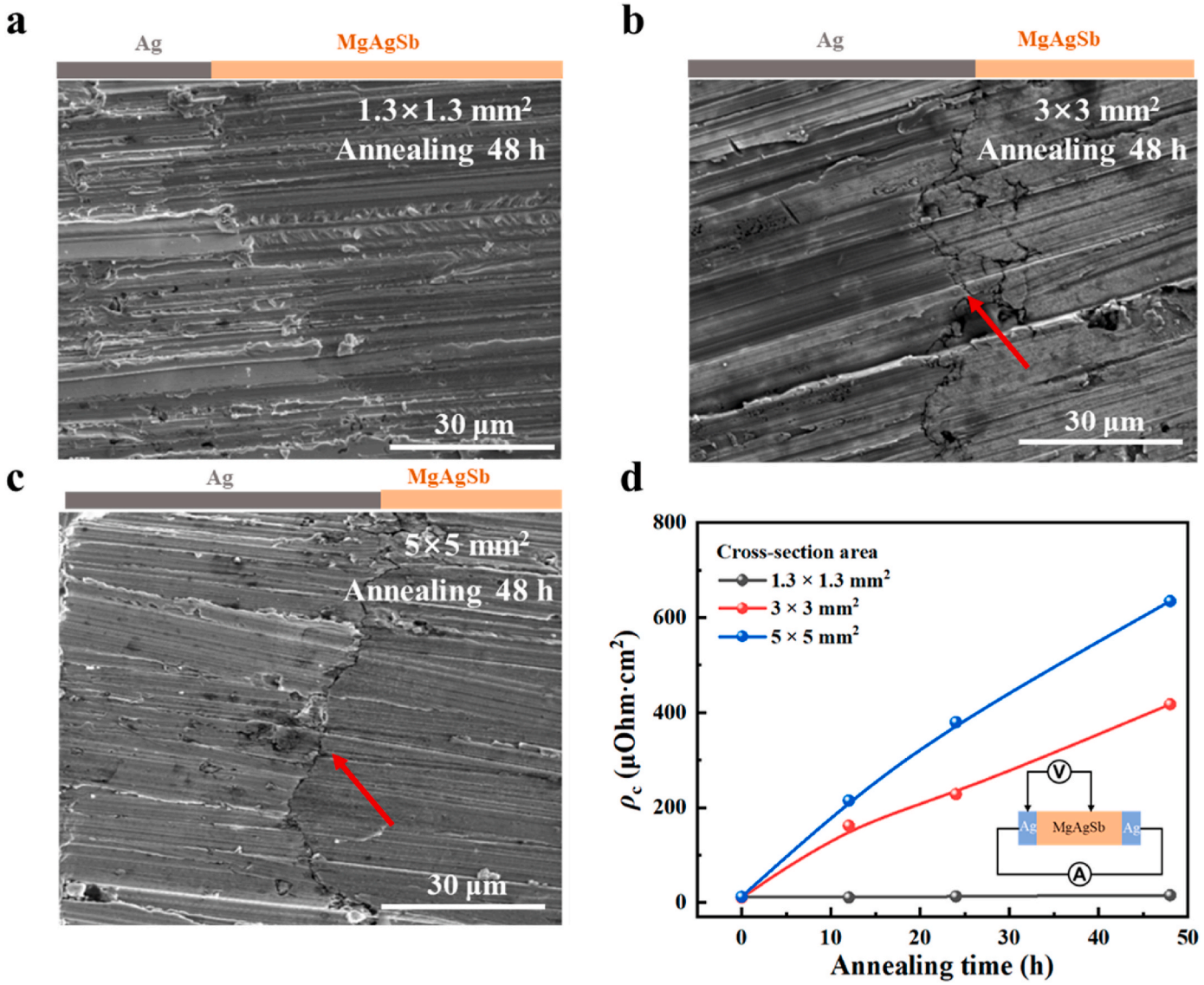

Fig. 4. The evolution of interfacial microstructure and contact resistivity. (a–c) SEM images of 48h-annealed MgAgSb/Ag junctions for different cross-sectional size legs. (d) Annealing time dependent interfacial resistivity of MgAgSb/Ag junctions for different cross-sectional size legs.

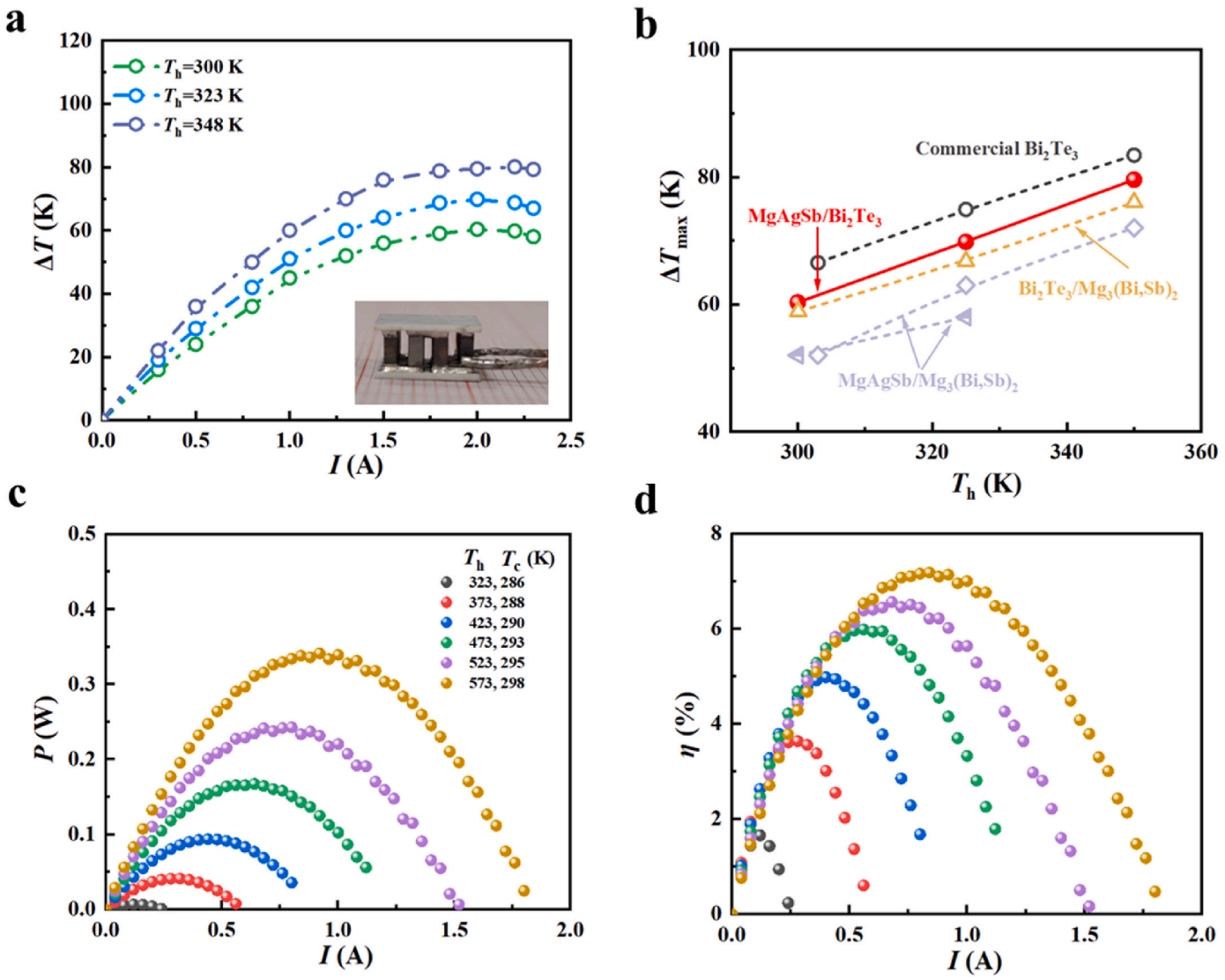

Fig. 5. Cooling and power generation performance of MgAgSb/Bi_2Te_3 TE modules. (a) Current dependent temperature difference ΔT, (b) ΔT_{max} as a function of hot-side temperature of MgAgSb/Bi_2Te_3 modules [34–36]. (c–d) Current dependent output power P and efficiency η under different temperatures for MgAgSb/-Bi_2Te_3 modules.

interplay among several effects, including Peltier effect, the Joule heat, thermal conduction and the Thomson effect. The decrease in ΔT under high current was attributed to the rapid increase in Joule heat. The measured maximum ΔT reached 60 K, 69 K and 80 K with the hot-side temperature at 300 K, 323 K and 348 K, respectively. Such an excellent cooling performance had exceeded most of the Mg-based cooling TE module and was comparable to the commercial Bi_2Te_3 cooling module [34–36] , as shown in Fig. 5b. The cooling efficiency, COP, which represents the amount of the heat pumped divided by the amount of supplied electrical power, was simulated with a hot-side temperature of 300 K in this work (Fig. S9). The simulated maximum COP of the MgAgSb/Bi_2Te_3 module increased from 2.3 to 8.1 for the temperature difference of 15 K–5 K.

Based on the excellent thermoelectric performance of the p-type MgAgSb material, we also characterized the power generation performance of the MgAgSb/Bi_2Te_3 module. Fig. 5c showed the current-dependent output power (P) of the MgAgSb/Bi_2Te_3 module under various temperature difference, which was obtained by the measured current-voltage curves (Fig. S10). As the current increases, the output power P initially raised and then declined, with the peak value corresponding to the matched impedance condition, where the internal resistance and load resistance were equal. At the working condition of $T_h = 573$ K and $T_c = 298$ K, the maximal output power of the module reached 0.34 W. Moreover, the current-dependent heat flow was measured as shown in Fig. S10, and subsequently the thermoelectric conversion efficiency (η) was evaluated based on the values, which showed a tendency similar to output power, as shown in Fig. 5d. Due to the Peltier effect and Joule heat, the optimal current of the maximizing efficiency differed from that of output power. A maximum efficiency (η_{max}) of 6 % was realized with the hot-side temperature of 523 K and the cold-side temperature of 295 K. The obtained efficiency exceeded most of the commercial Bi_2Te_3-based modules at the same temperature difference. However, the η_{max} only reached 7.2 % when the hot-side temperature increased to 573 K due to the performance deterioration of n-type Bi_2Te_3.

In summary, the α-MgAgSb demonstrated a remarkable thermoelectric performance attributed to its significant low lattice thermal conductivity of 0.58 W m^{-1} K^{-1}, stemming from its high atomic mass contrast and complex crystal structure. Within the temperature range of 150–300 K, MgAgSb achieved a zT_{avg} of 0.58, comparable to Bi_2Te_3, while in the range of 300–550 K, its zT_{avg} reached 1.22, substantially surpassing commercial Bi_2Te_3 material. Additionally, reducing the

cross-sectional size of the MgAgSb/Ag thermoelectric legs effectively prevented interface cracking during high-temperature operation. Based on the excellent thermoelectric properties and contact properties of the MgAgSb material, a 7-pair MgAgSb/Bi_2Te_3 thermoelectric modules was fabricated and evaluated for cooling and power generation. A maximum cooling temperature difference of 60 K was achieved at hot-side temperature of 300 K and a high power generation efficiency of 7.3 % was obtained with ΔT of 275 K. Benefit from the excellent performance of α-MgAgSb material and the module, we believed the Mg-based thermoelectric materials hold significant potential for thermoelectric applications in both cooling and power generation.

CRediT authorship contribution statement

Xiaofan Zhang: Writing – original draft, Visualization, Software, Methodology, Investigation, Formal analysis, Data curation. **Nan Chen:** Validation, Formal analysis, Data curation. **Kaiwei Guo:** Data curation. **Qintuo Zhang:** Software, Data curation. **Qi Zhao:** Data curation. **Jingkun Xu:** Data curation. **Hangtian Zhu:** Writing – review & editing, Project administration, Conceptualization. **Huaizhou Zhao:** Writing – review & editing, Validation, Supervision, Project administration, Funding acquisition.

Declaration of competing interest

The authors declare that they have no known competing financial interests or personal relationships that could have appeared to influence the work reported in this paper.

Data availability

Data will be made available on request.

Acknowledgments

The authors acknowledge the funding support of the National Key Research and Development Program of China (Grant No. 2018YFA0702100 and 2022YFB3803900) and the National Natural Science Foundation of China (Grant No. 52172262). This work is supported by the Research Platform of Material Genome and the Synergic Extreme Condition User Facility in Huairou, Beijing China.

Appendix A. Supplementary data

Supplementary data to this article can be found online at https://doi.org/10.1016/j.mtphys.2024.101451.

References

[1] L.E. Bell, Cooling, heating, generating power, and recovering waste heat with thermoelectric systems, Science 321 (2008) 1457–1461.
[2] J. Mao, G. Chen, Z. Ren, Thermoelectric cooling materials, Nat. Mater. 20 (2021) 454–461.
[3] G.J. Snyder, E.S. Toberer, Complex thermoelectric materials, Nat. Mater. 7 (2008) 105–114.
[4] J. Cao, et al., Thermoelectric device performance beyond average ZT: holistic consideration of materials and design, Mater. Today Phys. 34 (2023): 101071.
[5] T. Kanno, et al., Avoiding errors in efficiency measurements of high-performance thermoelectric generator modules: toward best practices for materials researchers, Mater. Today Phys. 36 (2023): 101171.
[6] Y. Qin, B. Qin, D. Wang, C. Chang, L.-D. Zhao, Solid-state cooling: thermoelectrics, Energy Environ. Sci. 15 (2022) 4527–4541.
[7] T. Zhu, et al., Compromise and synergy in high-efficiency thermoelectric materials, Adv. Mater. 29 (2017): 1605884.
[8] T. Lu, et al., Synergistically enhanced thermoelectric and mechanical performance of Bi2Te3 via industrial scalable hot extrusion method for cooling and power generation applications, Mater. Today Phys. 32 (2023): 101035.
[9] Z. Chen, et al., Lattice dislocations enhancing thermoelectric PbTe in addition to band convergence, Adv. Mater. 29 (2017): 1606768.
[10] Y. He, et al., Ultrahigh thermoelectric performance in mosaic crystals, Adv. Mater. 27 (2015) 3639–3644.
[11] A. Li, C. Fu, X. Zhao, T. Zhu, High-Performance $Mg_3Sb_{2-x}Bi_x$ Thermoelectrics: Progress and Perspective, vol. 2020, Research (Wash D C), 2020: 1934848.
[12] J. Callaway, Model for lattice thermal conductivity at low temperatures, Phys. Rev. 113 (1959) 1046–1051.
[13] M.G. Holland, Analysis of lattice thermal conductivity, Phys. Rev. 132 (1963) 2461–2471.
[14] E.S. Toberer, A. Zevalkink, G.J. Snyder, Phonon engineering through crystal chemistry, J. Mater. Chem. 21 (2011) 15843–15852.
[15] S.K. Bux, et al., Mechanochemical synthesis and thermoelectric properties of high quality magnesium silicide, J. Mater. Chem. 21 (2011): 12259.
[16] Q. Ren, et al., Establishing the carrier scattering phase diagram for ZrNiSn-based half-Heusler thermoelectric materials, Nat. Commun. 11 (2020) 3142.
[17] J. Li, et al., Thermal and electrical analysis of SiGe thermoelectric unicouple filled with thermal insulation materials, Appl. Therm. Eng. 134 (2018) 266–274.
[18] C. Fu, et al., Thermoelectric properties of FeVSb half-Heusler compounds by levitation melting and spark plasma sintering, Intermetallics 32 (2013) 39–43.
[19] Y. Pei, A. LaLonde, S. Iwanaga, G.J. Snyder, High thermoelectric figure of merit in heavy hole dominated PbTe, Energy Environ. Sci. 4 (2011) 2085–2089.
[20] G.E. Shoemake, J.A. Rayne, R.W. Ure, Specific Heat of n- and p-Type Bi_2Te_3 from 1.4 to 90°K, Phys. Rev. 185 (1969) 1046–1056.
[21] S. Lee, K. Esfarjani, J. Mendoza, M.S. Dresselhaus, G. Chen, Lattice thermal conductivity of Bi, Sb, and Bi-Sb alloy from first principles, Phys. Rev. B 89 (2014): 085206.
[22] Z. Liu, et al., Demonstration of ultrahigh thermoelectric efficiency of ~7.3% in Mg_3Sb_2/MgAgSb module for low-temperature energy harvesting, Joule 5 (2021) 1196–1208.
[23] B.C. Sales, B.C. Chakoumakos, R. Jin, J.R. Thompson, D. Mandrus, Structural, magnetic, thermal, and transport properties of$X_8Ga_{16}Ge_{30}$(X=Eu,Sr,Ba)single crystals, Phys. Rev. B 63 (2001): 245113.
[24] H. Zhao, et al., High thermoelectric performance of MgAgSb-based materials, Nano Energy 7 (2014) 97–103.
[25] Ionicity dependence of lattice thermal conductivity in tetrahedral semiconductors, Chem. Phys. Lett. 61 (1979) 542–544.
[26] Y. Kawaharada, K. Kurosaki, M. Uno, S. Yamanaka, Thermoelectric properties of $CoSb_3$, J. Alloys Compd. 315 (2001) 193–197.
[27] D.T.S. Morelli, G. A, High Thermal Conductivity Materials, Springer, New York, 2005.
[28] D.P. Spitzer, Lattice thermal conductivity of semiconductors: a chemical bond approach, J. Phys. Chem. Solid. 31 (1970) 19–40.
[29] D. Li, et al., Atomic disorders induced by silver and magnesium ion migrations favor high thermoelectric performance in α-MgAgSb-based materials, Adv. Funct. Mater. 25 (2015) 6478–6488.
[30] W.M. Yim, E.V. Fitzke, F.D. Rosi, Thermoelectric properties of Bi_2Te_3-Sb_2Te_3-Sb_2Se_3 pseudo-ternary alloys in the temperature range 77 to 300 K, J. Mater. Sci. 1 (1966) 52–65.
[31] N. Chen, et al., Improved figure of merit (z) at low temperatures for superior thermoelectric cooling in $Mg_3(Bi,Sb)_2$, Nat. Commun. 14 (2023) 4932.
[32] D. Kraemer, et al., High thermoelectric conversion efficiency of MgAgSb-based material with hot-pressed contacts, Energy Environ. Sci. 8 (2015) 1299–1308.
[33] L. Xie, et al., Screening strategy for developing thermoelectric interface materials, Science 382 (2023) 921–928.
[34] P. Ying, et al., Robust thermoelectric module based on MgAgSb/$Mg_3(Sb,Bi)_2$ with an 8.5% conversion efficiency and a 72 K maximum cooling, Energy Environ. Sci. 15 (2022) 2557–2566.
[35] L. Xie, et al., Highly efficient thermoelectric cooling performance of ultrafine-grained and nanoporous materials, Mater. Today 65 (2023) 5–13.
[36] J. Yang, et al., Next-generation thermoelectric cooling modules based on high-performance $Mg_3(Bi,Sb)_2$ material, Joule 6 (2022) 193–204.